Two-dimensional skyrmion lattice in a nanopatterned magnetic film

M. V. Sapozhnikov and O. L. Ermolaeva
Institute for Physics of Microstructures RAS, Nizhny Novgorod 603950, GSP-105, Russia
and N. I. Lobachevskii State University, Nizhny Novgorod 603950, Russia
(Received 4 April 2014; revised manuscript received 18 December 2014; published 20 January 2015)

We study the possibility of a two-dimensional (2D) skyrmion crystal stabilization in a magnetic film with perpendicular anisotropy in the absence of Dzyaloshinskii-Moriya interaction by creating the regular array of blind holes or stubs. By micromagnetic simulation we demonstrate that skyrmions can be stable in the patterned films with the parameters of ordinary materials such as CoPt, FePt, or FePd. The skyrmion lattices can be initialized in the system by simple magnetization in the uniform external magnetic field. At the zero external field the skyrmion helicity depends on the geometry of the blind hole or stub but also can be tuned by applying the field. The suggested method makes it possible to create dense enough (with the period less than 100 nm) skyrmion lattices which are important to carry out transport measurements.

DOI: 10.1103/PhysRevB.91.024418 PACS number(s): 75.70.Kw, 75.60.Jk

Recently it was theoretically predicted that magnetic states carrying topological charge can be stable in the chiral magnets without the assistance of an external magnetic field [1]. Very soon after that the prediction was experimentally verified by the observation of such structures by neutron scattering (in MnSi) [2], by Lorentz transmission electron microscopy (in $Fe_{0.5}Co_{0.5}Si$) [3], and by spin-resolved scanning tunneling microscopy (hexagonal Fe monolayer) [4]. Since these pioneering works such magnetic structures are usually referred to as "magnetic skyrmions." The rising interest to magnetic skyrmions is caused by discovering their unusual spin-electronic properties, such as the topological Hall effect [5,6], current-driven motion in ultralow currents [7] accompanied by skyrmion Hall effect [8], or flexomagnetoelectric effects [9] which can be exploited in spintronic devices. The skyrmion lattice is stabilized by Dzyaloshinskii-Moriya (DM) interaction [10,11] in these materials. The problem is that the relativistic DM interaction is commonly weak so the magnetic skyrmion lattice can be stable within a narrow temperature and magnetic field range in some noncentrosymmetric materials (see Table 1 from Ref. [12]).

In principle it is known that the existence of skyrmionlike magnetization distribution is possible in materials without the DM interaction. As an example, magnetic bubble domains in YIG film being in the external field [12] or domains obtained by heat-assisted magnetic recording in FePd films [13] can be mentioned. Although bubble domains in YIG are topologically magnetic skyrmions, their large size leads to low average skyrmion density defined as [2]

$$\phi = \frac{1}{4\pi}\mathbf{n}\cdot\frac{\partial \mathbf{n}}{\partial x}\times\frac{\partial \mathbf{n}}{\partial y}, \tag{1}$$

$\mathbf{n} = \mathbf{M}(\mathbf{r})/|\mathbf{M}(\mathbf{r})|$ is the orientation of the magnetization. Also the nonconductive nature of the material makes it impossible to observe such a system of transport effects. So at the moment there is no method of creating skyrmion arrays in conventional conductive ferromagnetic materials with a skyrmion charge density sufficient to experimentally observe unique transport effects caused by the skyrmion topology.

Recently they suggested creating a 2D skyrmion lattice in CoPt film with perpendicular anisotropy by placing Co particles on its surface and corroborated this approach by micromagnetic simulation [14]. The idea was that the magnetic vortex within the Co particles will stabilize skyrmionlike magnetization distribution in the CoPt film below it due to exchange interaction between the film and the particles. This method involves the lithography of the asymmetric cobalt dots such as edge-cut circular disks or polygonal dots. Such shape of the dots is necessary to have the possibility that all of the magnetic vortices in the particles get the same chirality during the magnetization in the uniform external field. In the actual experiments the size of such particles is 1–2 μm [15,16]. According to our own experience the smallest size of the triangular particles (arranged in the 2D lattice) suitable for obtaining the vortices with the same chirality is about 500 nm [17]. This limits the density of the 2D skyrmion lattice in such a system by approximately 1 μm^{-2}.

In this paper we want to suggest an alternative method of nanopatterning of the magnetic film with perpendicular anisotropy (CoPt, FePt, FePd) which will enable to create 2D skyrmion lattice with more than 100 times higher skyrmion charge density. Wherein the skyrmion lattice can be initialized by the simple magnetizing in the uniform magnetic field. Our idea is that it is possible to prevent skyrmion collapse (radial instability) and runout (elliptic instability) by periodically changing the film thickness. If the magnetic bubble (topologically it is a magnetic skyrmion) is initially in the thin area of the film its runout will cause not only the increase of the domain wall length (like in the case of flat film) but the domain wall height (i.e., size in the normal to film direction) will increase as well as the domain wall shifts into the region where the film has a greater thickness. This will lead to the additional increase of free energy of the system and so runout can be prevented. In the case of very thin perpendicular magnetic films, those thickness are less than some critical value [18], the magnetic bubble is also unstable but has the tendency to squeeze and collapses. In this case the local thickening of the film located in the middle of the bubble domain can stop the squeeze due to the same mechanism. So the regular array of the circular blind holes or stubs can play the role of a matrix which can stabilize the skyrmion lattice (bubble domains) without need of DM interaction. The suggested method of the nanopatterning has the evident advantages.

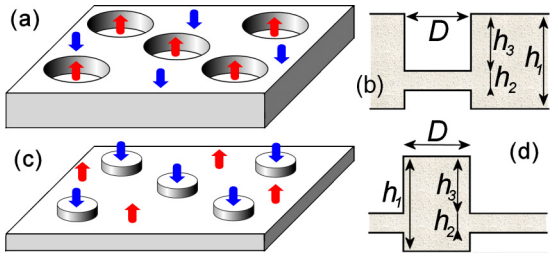

FIG. 1. (Color online) The geometry of the proposed skyrmion system. (a) The regular array of the blind holes, arrows denote the direction of the magnetization inside and outside the blind holes in the presence of the skyrmion lattice. (b) The cross section of the blind hole, the geometry parameters used in micromagnetic simulations are shown: h_1 is the thickness of the initial film, D is the diameter of the blind hole, h_2 is the thickness of its bottom, and h_3 is its depth. (c) The regular array of the stubs. (d) Corresponding geometrical parameters.

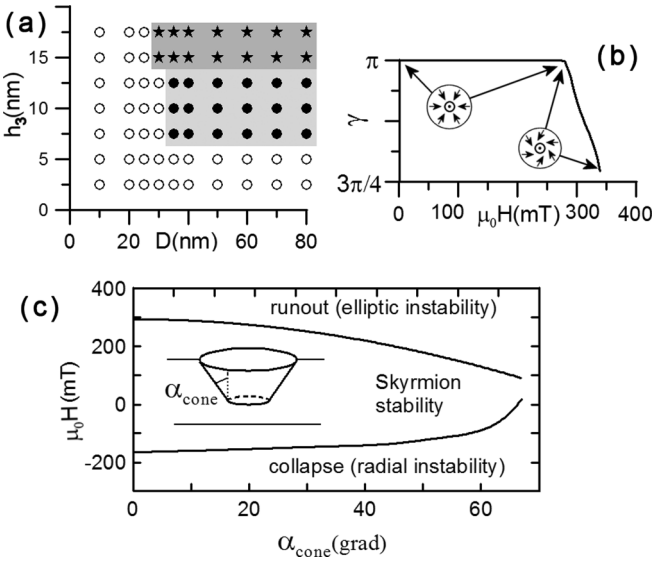

FIG. 2. (a) Calculated phase diagram for the skyrmion stability in the blind hole (see Fig. 1 for the geometry parameters, $h_1 = 20$ nm, $h_1 = h_2 + h_3$). The stars shows the skyrmion with the helicity $\gamma = \pi$, solid circles represent skyrmion with the helicity $\gamma < \pi$, and open circles are for the skyrmion instability. (b) The dependence of the helicity of the skyrmion in the blind hole ($h_1 = 30$ nm, $h_2 = 5$ nm, $h_3 = 25$ nm, and $D = 40$ nm) on the external magnetic field. (c) The external field range when the skyrmion is stable in the conical blind hole depending on the cone slope, $h_1 = 20$ nm, $h_3 = 15$ nm, the average cone diameter is 50 nm.

(1) It is possible to lithography the lattice of holes or stubs with diameters less than 20 nm [19], this can essentially increase the density of the artificial skyrmion lattice.

(2) The skyrmion lattice can be formed easily by magnetizing the sample in the external uniform field, it is possible to manipulate the density and even the symmetry of the skyrmion lattice in the same sample by changing the value of the applied field. Wherein the obtained skyrmion lattices remain stable at the zero field.

(3) It is possible to obtain the skyrmions with different helicity by changing the geometry of the blind hole or stub.

(4) It is possible to manipulate the skyrmion parameters such as diameter or helicity by applying the external field.

We verify the suggested approach with micromagnetic simulations utilizing the OOMMF code [20] based on a numerical solution of the system of Landau-Lifshitz-Gilbert (LLG) equations for the magnetization of the system. The geometry of the simulated system is represented in Fig. 1. Actually it is the regular hexagonal or square array of the blind holes. They are characterized by diameter and thickness parameters h_1, h_2, and h_3. In most of the calculations $h_1 = h_2 + h_3$, so h_1 is the film thickness, h_2 is the blind hole bottom thickness, and h_3 is its depth. The parameters of the stub are similar. It is known that depending on the chemical composition the material parameters of the magnetic perpendicular medium are varied within certain limits: $M_s = 5 \times 10^5/13 \times 10^5$ A/m, $A = 10^{-11}/1.5 \times 10^{-11}$ J/m, and $K_u = 4 \times 10^5/10^7$J/m^3 (it is the saturated magnetization, exchange coefficient, and uniaxial anisotropy) [14,21–26]. For our simulations we used values within this range. At the first stage we study the possibility of the single skyrmion stabilization in the blind holes of different geometries "drilled" in the center of a 300×300 nm fragment of the 20 nm thick plane film. A grid size is $2.5 \times 2.5 \times 2.5$ nm^3. A starting point for the calculations is uniformly magnetized film ($M_z = -M_s$) with the blind hole bottom magnetized oppositely ($M_z = M_s$) and after that the system relaxes in a stationary state. The phase diagram at zero external field for $M_s = 8 \times 10^5$ A/m, $A = 10^{-11}$ J/m, and $K_u = 5 \times 10^6$J/m^3 is represented in Fig. 2(a). In the case of the deep blind hole the skyrmion has helicity $\gamma = \pi$ (or $\gamma = 0$ for the opposite initial orientation of the magnetization). In the case of the shallow blind hole the skyrmion obtains some azimuthal component. If the blind hole is too shallow ($h_3 = 5$ nm) or narrow ($D = 25$ nm) the skyrmion has elliptical instability and the reversed domain spreads over the film. It is necessary to mention that the magnetic moment distribution of similar skyrmionlike structure can be obtained in the magnetic nanodisk with perpendicular anisotropy whose size is slightly larger than single-domain size. In this case the bubble domain is stabilized due to the small enough size of the particle, there is no room to form labyrinth structure [27].

To understand how precise technology must be in terms of manufacturing of blind holes we check the stability of the skyrmions in the holes with inclined edges. The results for the blind conical holes are represented in Fig. 2(c) for the 20 nm thick film with material parameters same as above. It demonstrates that skyrmions stay stable at zero external fields up to high enough inclination angles while the corresponding range of the external fields gradually narrows.

Using the same procedure we study the stability of the skyrmion pinned by a cylindrical stub on the surface of a 5 nm thick film. This thickness is less than the critical value (8 nm for the used material parameters) when the magnetic bubble topologically similar to the skyrmion is radially unstable (i.e., collapses) even at the zero external field [18]. So a skyrmionlike nucleus collapses in the flat film or if the stub diameter or height is too small [Fig. 3(b)]. If the stub is higher the initial skyrmion nucleus shrinks while its diameter reaches the diameter of the stub. After that it remains stable.

K=5*10^5J/m^3

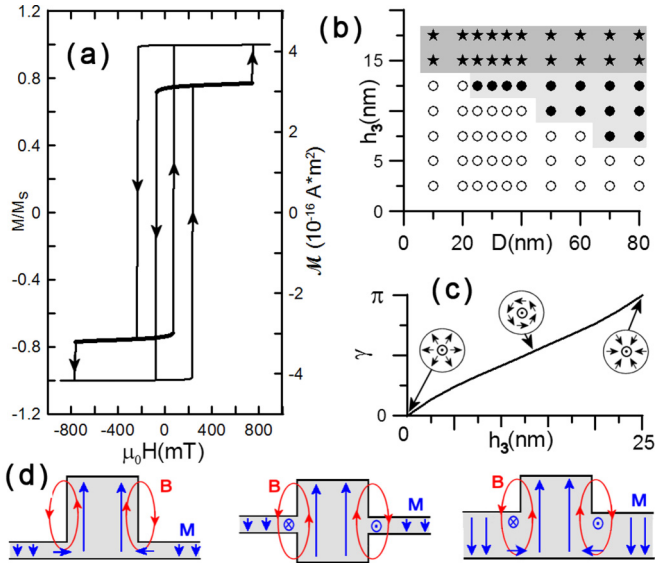

FIG. 3. (Color online) (a) The magnetization curve in the perpendicular magnetic field for the 300 nm × 300 nm × 30 nm plate with the stub ($D = 50$ nm, $h_3 = 25$ nm) in the center. Left graph axis shows the absolute value of the magnetic moment of the system. The thick parts of the curve correspond to the skyrmionlike magnetization distribution in the stub. (b) Calculated phase diagram for the skyrmion stability of the stub (see Fig. 1 for the geometry parameters, $h_1 = 20$ nm, $h_1 = h_2 + h_3$). The stars shows the skyrmion with the helicity $\gamma = \pi$, solid circles represent skyrmion with the helicity $\gamma < \pi$, and open circles are for the skyrmion instability. (c) The dependence of the skyrmion helicity in the stub ($h_1 = 30$ nm, $h_2 = 5$ nm) on the relative position of the film and stub in the general case ($h_1 \neq h_2 + h_3$) for the zero external field. (d) The scheme of the demagnetizing fields and magnetization distribution for different geometries of the system.

The hysteresis magnetization curve of the system is represented in Fig. 3(a). The skyrmion stays stable in the wide range of the external field values. It becomes radially unstable at the field $\mu_0 H = 740$ mT when its core collapses and becomes elliptically unstable at $\mu_0 H = -70$ mT, causing magnetization reversal in the whole system. The magnetic moment $\mathcal{M}$ associated with the skyrmion core is approximately equal in this case to 2×10^{-16} A m^2. This allows us to understand the possible influence of the thermal fluctuations on the skyrmion stability at room temperature. The energy barrier responsible for the stability of the skyrmion at zero field can be estimated as $\Delta E = \mu_0 H \mathcal{M}$, where $\mu_0 H \sim 10^{-1}$ T is a field of the skyrmion instability. So the corresponding energy is $\sim 10^{-17}$ J and the corresponding temperature 10^6 K which is more than three orders higher than the Curie temperature of the material and more than three orders higher than room temperature. So the influence of the temperature fluctuations on the skyrmion stability is negligible in the system.

The helicity of the skyrmion is determined by demagnetizing field configurations and so depends on the geometry of the system [Figs. 3(c) and 3(d)]. For the system with the flat bottom surface (i.e., $h_1 = h_2 + h_3$) if h_2 is smaller than the exchange length ($h \lesssim 5$ nm) the skyrmion has the helicity $\gamma = 0, \pi$ (pure Néel type). For the thicker h_2 the helicity becomes nonuniform in the vertical direction [Fig. 3(d)]. The same situation is observed for the skyrmion in the blind hole. So by varying the geometry of the system it is possible to obtain the skyrmions with the different helicity numbers. Moreover, our simulations demonstrate that the skyrmion can be manipulated by applying the uniform external magnetic field. If the applied field is directed against its core magnetization it begins to shrink, vice versa if the field is the same direction and the skyrmion core widens [Fig. 5(c)]. This takes place until it does not lose its stability. The widening is accompanied by a change in its skyrmion helicity [Fig. 2(b)]. It is necessary to note that the micromagnetic simulations confirm the possibility of the skyrmion stabilization in the blind hole or on the stub in the wide range of the material parameters (mentioned above) with proper geometrical configuration of the system.

At the second stage of our study we investigate the possibility of the skyrmion lattice formation in the initially uniformly magnetized system by applying an external magnetic field. The condition of numerical simulations is slightly changed in this case. The calculation is done for a 640 × 640 × 30 nm piece of the 30 nm thick magnetic film which contains 23 hexagonally arranged blind holes. Their diameter and depth are 60 nm and 25 nm, and the lattice period is 110 nm. We especially do not use the periodical boundary conditions to take into account possible boundary effects which for sure can take place in the real experiment. Also we slightly (2.5 nm) shift the array of the blind holes relative to the center of the system to reduce its symmetry. The used material parameters are $M_s = 9 \times 10^5$ A/m, $A = 10^{-11}$ J/m, and $K_u = 7 \times 10^6$J/m^3. Starting with the 7*10^5 uniformly perpendicularly magnetized system we calculate the magnetization hysteresis loop. It is presented in Fig. 4 in detail. The magnetization process takes place as follows. If the field is directed opposite to the initial magnetization of the system it remains stable till $\mu_0 H = 164$ mT [point D in Figs. 4(a)–4(c)]. After that the reversal of the first blind hole takes place and the skyrmion is formed in it. Due to the effective antiferromagnetic character of the magnetostatic interaction between skyrmion cores an additional field is necessary to reverse the second blind hole and initialize skyrmion in it. So the magnetization process receives step-by-step character and the magnetization curve has a form of devil staircase, when the narrow steps are between the wider ones [Fig. 4(c)]. The wider steps correspond to the formation of more symmetrical arrays of skyrmions [Fig. 4(b)]. This stage of the reversal process ends at 204 mT with the formation of the dense skyrmion lattice [Fig. 4(a)]. The lattice stay stable in the wide range of the fields (-225 mT $< \mu_0 H <$ 500 mT). If the field becomes less than -225 mT (point B) the reverse process is observed when the skyrmions one-by-one shrink and disappear. This part of the curve has also a devil-staircase-like shape. If the field becomes larger than 500 mT one of the skyrmions become elliptically unstable, reversed domain spreads through the whole system, and it becomes uniformly magnetized. Remarkably it is possible to stop the magnetization process at any place on the devil staircase between points D and A, and so create the skyrmion lattice with the desired symmetry which is stable in the wide field ranges [Fig. 4(b)]. By applying the appropriate external field it is possible to switch the system between these states.

Let us estimate the influence of the thermal fluctuations on the tiny structure of the devil-staircase branch of the

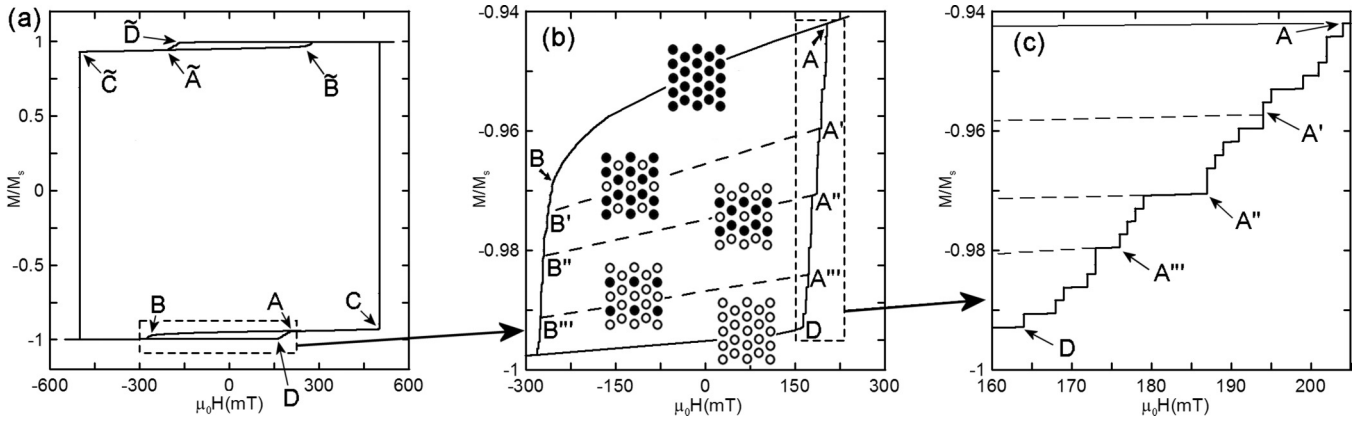

FIG. 4. The typical magnetization curve of the hexagonal array (the period is 110 nm) of the blind holes (the diameter is 60 nm, the depth is 25 nm) in 30 nm thick film. (b) Close view of the part of the magnetization curve showing the range of the stability of the skyrmion lattices with different symmetries. The black circles represents blind holes with reversed magnetization, i.e., skyrmions. (c) The devil-staircase-like shape of the magnetization curve caused by the effective antiferromagnetic magnetostatic interaction between skyrmions.

magnetization curve. The energy barrier between the different skyrmion lattices on the same nanostructured matrix which causes the appearance of the steps on the curve has the order of $\Delta E \sim \mu_0 \Delta H \mathcal{M}$, where $\mathcal{M} \sim 10^{-16}$ A m^2 is the skyrmion core magnetic moment and $\mu_0 \Delta H$ is the width of the corresponding step on the curve. Comparing this energy with the energy of the fluctuations at room temperature it is possible to find some critical value of the step width which is $\mu_0 \Delta H_c \sim k_B T/\mathcal{M} \sim 3 \times 10^{-5}$ T $= 3 \times 10^{-1}$ Oe. So this is the minimal width of the step which can be resolved experimentally at room temperature, more narrow steps will be blurred due to the thermal fluctuations.

On the other hand, it is interesting to compare $k_B T$ with the energy of the magnetostatic interaction between the skyrmion cores, which is $E = \mu_0 \mathcal{M}^2/4\pi r^3$ in dipole-dipole approximation. This way it is possible to find the distance between two skyrmions at which their magnetostatic interaction begins to exceed the thermal fluctuations. It is about 1 μm. It means that the steps on the magnetization curves related to the complex skyrmion lattices with the periods less than this critical distance will be resolved, while the narrow steps correspond to the complex skyrmion lattices with periods larger than 1 μm will be blurred at room temperature. Let as stress one more time that we discuss here the different skyrmion lattices that can be realized on the *same* matrix of the blind holes during the magnetization [Fig. 4(b)]. The nature of the devil-staircase-like magnetization curves in systems with effective antiferromagnetic interaction even at nonzero temperatures is discussed in Ref. [28] in detail.

To explore topological properties of obtained skyrmion lattice, we calculated the distribution of the local skyrmion density in the lattice (1) [Fig. 5(b)]. For the different values of the external magnetic field the maximal skyrmion density is changed from $\phi = -6.63$ nm^{-2} at $\mu_0 H = 500$ mT to $\phi = -8.9$ nm^{-2} at $\mu_0 H = -255$ mT as the skyrmion changes its diameter. Nevertheless, the skyrmion number calculated as the integral of the skyrmion density over the lattice cell is always equal to -1 between B and C points of the magnetization curve. Evidently for the opposite direction of the cores (between $\tilde{\text{B}}$ and $\tilde{\text{C}}$ points) the skyrmion number is equal to 1. In principal the skyrmions are observed while magnetizing the lattice of the blind holes for the different values of the material parameters within the range mentioned above as usual for perpendicular magnetic media. But for the arbitrary material parameters the part of the blind hole turned to be in the C states. Nevertheless, it is possible to choose such material parameters or system geometry when C states become unstable according to its transformation in the skyrmion. The material parameters which are used to calculate magnetization curves represented in Figs. 4 and 6 satisfy the condition.

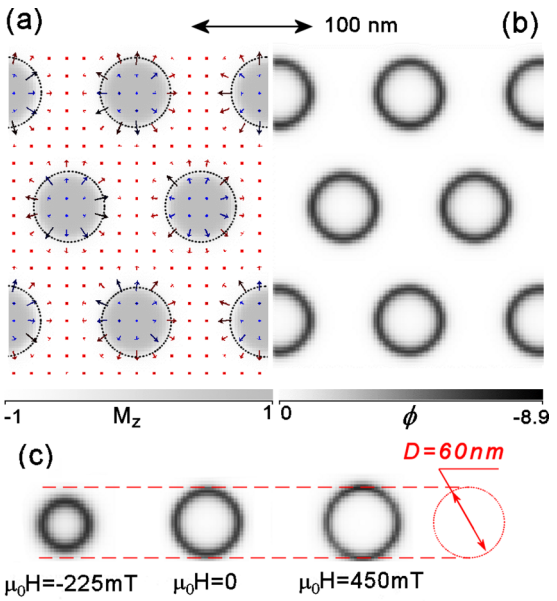

FIG. 5. (Color online) (a) Magnetization distribution in the skyrmion lattice on the blind hole array at $H = 0$, part of the simulated system is shown. Dotted lines denote the blind hole edges. (b) Calculated local skyrmion density ϕ per unit cell for the same skyrmion lattice. (c) The dependence of the skyrmion density ϕ distribution on the external magnetic field. The red circle denotes the size of the blind hole, $D = 60$ nm.

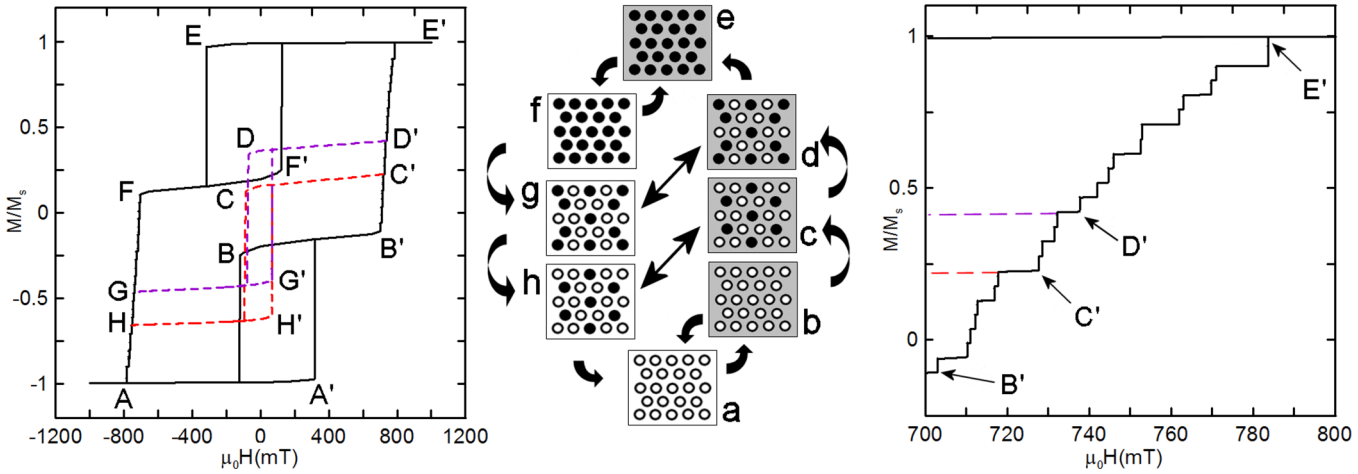

FIG. 6. (Color online) Left: The typical magnetization curve of the hexagonal array (the period is 120 nm) of the cylindrical stubs (the diameter is 60 nm, the height is 25 nm) on the surface of the 5 nm thick film. Pairs of the capital letters A-A′, B-B′, C-C′, etc. indicate the ranges of the stability of the skyrmion lattices denoted by the same lowercase letters a, b, c which are schematically represented in the middle. Middle: Some (the most symmetrical) of the possible skyrmion lattices consequently arising during the magnetization of the array of the stubs. The black color (for the stubs) and gray color (for the film) denote the up-directed magnetization, the white is for down-magnetized regions of the system. The arrows indicate the possible transitions between the states caused by applied external field. Right: The devil-staircase-like shape of the magnetization curve between B′ and E′ is presented.

The magnetization curve of hexagonal lattice of the stabs ($D = 60$ nm, $h_3 = 25$ nm, period 120 nm) on the 600×600 nm and 5 nm thick pedestal is shown in Fig. 6. In this case the magnetization reversal begins in the thin base film. At $\mu_0 H = 318$ mT the nucleus with the reversed magnetization appears and the reversed domain spread through all the pedestal. Even so the stubs keep their magnetization unreversed at this field value. So the formation of the dense hexagonal array (state "b" in the scheme in Fig. 6) occurs. This skyrmion lattice remains stable in the wide range of the external field values (points B and B′ in Fig. 6). At the field value larger than 704 mT the dense skyrmion lattice become unstable and successive reversal of the stubs was observed with the further increase of the external field. The reversal ends at 786 mT (point E′). This part of the magnetization curve has the devil-staircase-like shape similar to that shown in Fig. 4(c) for the blind hole lattice. During the reversal the system passes through the sequence of states which have different numbers of skyrmions. Some of the most symmetric states are presented in Fig. 6. By applying the uniform external field it is possible to obtain different stable skyrmion lattices and also switch the system between these stable states.

To finish with we should make some remarks.

(1) We checked and made sure that the exact cylindrical shape of the blind hole or stub is not necessary for skyrmion stabilization. The elliptical or conical shape is also suitable, as the stabilization mechanisms work in the same way in these cases.

(2) It is well known that the coercivity of the perpendicular magnetic films can be significantly less than anisotropy. The magnetization reversal can start with the appearance of the reversed nucleus in the "weak" place in this case. Our calculations demonstrate that the bottom of the blind hole or pedestal in the lattice of stabs is naturally such a weak place (due to the specifics of the demagnetizing field distribution in the system), where the nucleus appears at fist. The existence of the additional weak places such as related to polycrystal structure of the initial film can shift the specific fields of the magnetization loop of the system but will not significantly change.

(3) Evidently if we apply an electric current to the system it will have the tendency to flow in the thicker parts of the patterned film. Therefore, it will avoid the blind hole bottoms and vise versa will be concentrated in the stubs. So the unique transport effects related to skyrmions will be more pronounced in the lattice of the stubs than in the lattice of the blind holes.

So we suggest the method for creating a 2D artificial lattice of magnetic skyrmions by lithographic patterning of the perpendicular magnetic film. Wherein the skyrmion charge density can be more than $100/\mu m^2$. By numerical simulations we demonstrate how such a lattice can be formed in the simple process of the magnetization in the uniform external field.

This research is supported by the Russian Foundation for Basic Research (RFBR) and by The Ministry of education and science of the Russian Federation (Agreements No. 02.B.49.21.0003 and No. 14.578.21.0041 with the Lobachevsky State University of Nizhny Novgorod).

[1] U. K. Rossler, N. Bogdanov, and C. Pleiderer, Nature (London) **442**, 797 (2006).

[2] S. Muhlbauer, B. Binz, F. Jonietz, C. Pfleiderer, A. Rosch, A. Neubauer, R. Georgii, and P. Boni, Science **323**, 915 (2009).

[3] X. Z. Yu, Y. Onose, N. Kanazawa, J. H. Park, J. H. Han, Y. Matsui, N. Nagaosa, and Y. Tokura, Nature (London) **465**, 901 (2010).
[4] S. Heinze, K. von Bergmann, M. Menze, J. Brede, A. Kubetzka, R. Wiesendanger, G. Bihlmayer, and S. Blugel, Nat. Phys. **7**, 713 (2011).
[5] Y. Onose, N. Takeshita, C. Terakura, H. Takagi, and Y. Tokura, Phys. Rev. B **72**, 224431 (2005).
[6] A. Neubauer, C. Pfleiderer, B. Binz, A. Rosch, R. Ritz, P. G. Niklowitz, and P. Boni, Phys. Rev. Lett. **102**, 186602 (2009).
[7] F. Jonietz, S. Muhlbauer, C. Pfleiderer, A. Neubauer, W. Munzer, A. Bauer, T. Adams, R. Georgii, P. Boni, R. A. Duine, K. Everschor, M. Garst, and A. Rosch, Science **330**, 1648 (2010).
[8] J. Zang, M. Mostovoy, J. H. Han, and N. Nagaosa, Phys. Rev. Lett. **107**, 136804 (2011).
[9] A. K. Zvezdin and A. P. Pyatakov, Phys.-Usp. **52**, 845 (2009).
[10] I. Dzyaloshinsky, J. Phys. Chem. Solids **4**, 241 (1958).
[11] T. Moriya, Phys. Rev. **120**, 91 (1960).
[12] N. Nagaosa and Y. Tokura, Nat. Nanotech. **8**, 899 (2013).
[13] W. A. Challener, C. Peng, A. V. Itagi, D. Karns, W. Peng, Y. Peng, X. Yang, X. Zhu, N. J. Gokemeijer, Y.-T. Hsia, G. Ju, R. E. Rottmayer, M. A. Seigler, and E. C. Gage, Nat. Photon. **3**, 220 (2009).
[14] L. Sun, R. X. Cao, B. F. Miao, Z. Feng, B. You, D. Wu, W. Zhang, A. Hu, and H. F. Ding, Phys. Rev. Lett. **110**, 167201 (2013).
[15] S. Yakata, M. Miyata, S. Nonoguchi, H. Wada, and T. Kimura, Appl. Phys. Lett. **97**, 222503 (2010).
[16] R. K. Dumas, T. Gredig, C.-P. Li, I. K. Schuller, and K. Liu, Phys. Rev. B **80**, 014416 (2009).
[17] O. G. Udalov, M. V. Sapozhnikov, E. A. Karashtin, B. A. Gribkov, S. A. Gusev, E. V. Skorohodov, V. V. Rogov, A. Yu. Klimov, and A. A. Fraerman, Phys. Rev. B **86**, 094416 (2012).
[18] Equation (4.9) in T. H. O'Dell, *Ferromagnetodynamics. The Dynamics of Magnetic Bubbles, Domains and Domain Walls* (MacMillan, New York, 1981).
[19] S. Ishio, S. Takahashi, T. Hasegawa, A. Arakawa, H. Sasaki, Z. Yan, X. Liu, Y. Kondo, H. Yamane, J. Ariake, M. Suzuki, N. Kawamura, and M. Mizumaki, J. Magn. Magn. Mater. **360**, 205 (2014).
[20] M. J. Donahue and D. G. Porter, *OOMMF User's Guide Version 1.0* (National Institute of Standards and Technology, Gaithersburg, MD, 1999).
[21] K. Barmak, J. Kim, L. H. Lewis, K. R. Coffey, M. F. Toney, A. J. Kellock, and J.-U. Thiele, J. Appl. Phys. **98**, 033904 (2005).
[22] M. Yu, H. Ohguchi, A. Zambano, I. Takeuchi, J. P. Liu, D. Josell, and L. A. Bendersky, Mater. Sci. Eng. B **142**, 139 (2007).
[23] M. Maret, M. C. Cadeville, R. Poinsot, A. Herr, E. Beaurepaire, and C. Monier, J. Magn. Magn. Mater. **166**, 45 (1997).
[24] S. Okamoto, N. Kikuchi, O. Kitakami, T. Miyazaki, Y. Shimada, and K. Fukamichi, Phys. Rev. B **66**, 024413 (2002).
[25] V. Gehanno, A. Marty, B. Gilles, and Y. Samson, Phys. Rev. B **55**, 12552 (1997).
[26] R. F. C. Farrow, D. Weller, R. F. Marks, M. F. Toney, A. Cebollada, and G. R. Harp, J. Appl. Phys. **79**, 5967 (1996).
[27] S. Komineas, C. A. F. Vaz, J. A. C. Bland, and N. Papanicolaou, Phys. Rev. B **71**, 060405(R) (2005).
[28] A. A. Fraerman and M. V. Sapozhnikov, Phys. Rev. B **65**, 184433 (2002).